

Article

Solution-Processable Benzo[*b*]thieno[2,3-*d*]thiophene Derivatives as Organic Semiconductors for Organic Thin-Film Transistors

Seongyun Kim ^{1,†}, Soomin Ryu ^{2,†}, Jihae Ahn ², Dongkyu Kim ³, Assunta Marrocchi ⁴ , Choongik Kim ^{1,*} and SungYong Seo ^{2,5,*}

¹ Department of Chemical and Biomolecular Engineering, Sogang University, Seoul 04107, Republic of Korea; ksy99791551@gmail.com

² Department of Smart Green Technology Engineering, Pukyong National University, Busan 48513, Republic of Korea; soomin009@naver.com (S.R.); fks0409@naver.com (J.A.)

³ Advanced Materials Division, Korea Research Institute of Chemical Technology (KRICT), Daejeon 34114, Republic of Korea; kdongkyu@kRICT.re.kr

⁴ Department of Chemistry, Biology and Biotechnology, University of Perugia, Via Elce di Sotto, 8, 06123 Perugia, Italy; assunta.marrocchi@unipg.it

⁵ Department of Chemistry, Pukyong National University, Busan 48513, Republic of Korea

* Correspondence: choongik@sogang.ac.kr (C.K.); syseo@pknu.ac.kr (S.S.)

† These authors contributed equally to this work.

Abstract: Two new benzo[*b*]thieno[2,3-*d*]thiophene (BTT) derivatives, 2-(benzo[*b*]thiophen-5-yl)benzo[*b*]thieno[2,3-*d*]thiophene (compound **2**), and 2-(benzo[*b*]thieno[2,3-*d*]thiophene-2-yl)dibenzo[*b,d*]thiophene (compound **3**) have been synthesized and utilized as solution-processable small molecular organic semiconductors for organic field-effect transistors (OFETs). The physicochemical characteristics of the recently created substances were analyzed using thermogravimetric analysis (TGA), differential scanning calorimeter (DSC), and UV-vis spectroscopy. Subsequently, the above-mentioned substances were employed as semiconductor layers in bottom-gate/top-contact OFETs through solution shearing methods for device fabrication, and their electrical performances were meticulously evaluated. The outcoming OFET device displayed p-channel behavior, demonstrating hole mobility of up to 0.005 cm²/Vs and a current on/off ratio higher than 10⁶.

Keywords: organic thin film transistors; organic semiconductor; benzo[*b*]thieno[2,3-*d*]thiophene; solution process



Citation: Kim, S.; Ryu, S.; Ahn, J.; Kim, D.; Marrocchi, A.; Kim, C.; Seo, S. Solution-Processable Benzo[*b*]thieno[2,3-*d*]thiophene Derivatives as Organic Semiconductors for Organic Thin-Film Transistors. *Coatings* **2023**, *13*, 1417. <https://doi.org/10.3390/coatings13081417>

Academic Editor: Alexandru Enescu

Received: 9 June 2023

Revised: 31 July 2023

Accepted: 4 August 2023

Published: 12 August 2023



Copyright: © 2023 by the authors. Licensee MDPI, Basel, Switzerland. This article is an open access article distributed under the terms and conditions of the Creative Commons Attribution (CC BY) license (<https://creativecommons.org/licenses/by/4.0/>).

1. Introduction

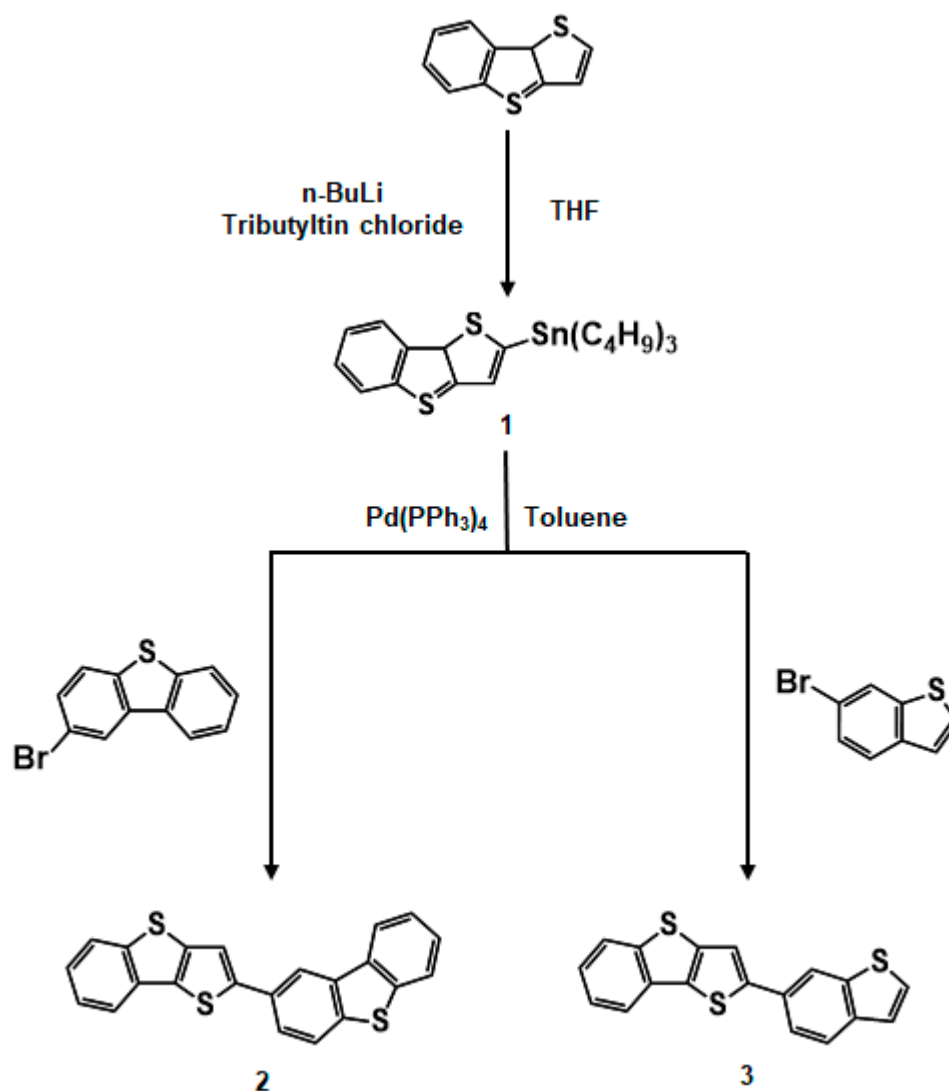
Organic semiconductors (OSCs) have attracted considerable attention for their potential application in a range of electronic appliances thanks to their desirable characteristics, inclusive of cost-effective fabrication, the capability to be processed at low temperatures over large areas, and flexibility [1–8]. In particular, organic semiconductors have been utilized in several electronic appliances, inclusive of organic field-effect transistors (OFETs), organic photovoltaics (OPVs), organic light-emitting diode (OLED) displays, optical sensors, and radio-frequency tags [9–17].

There are two major deposition methods for fabricating thin films of organic semiconductors: vacuum or solution process. Despite the fact that semiconductors devised for vacuum vapor deposition generally exhibit high field-effect mobility, they have several drawbacks. The main issues with the vacuum deposition method are its high cost and the difficulty of large-area processing. Additionally, it requires a relatively long processing time and high temperature [18,19]. Therefore, the solution process has risen as a highly promising substitute for the vacuum process, offering cost-effectiveness, low-temperature, and large-scale manufacturing [20,21].

Great endeavors have been dedicated to the advancement of OSCs with exceptional electrical performance as well as enhanced air stability [22–26]. In particular, π -conjugated small-molecule organic semiconductors have received significant attention compared to polymeric materials due to their relative ease of synthesis and improved reproducibility, solubility, and purity [27–32]. For instance, small-molecule OSCs based on oligothiophene, tetracene, pentacene, and acene derivatives have demonstrated impressive electrical performance and excellent air stability.

Fused thiophenes are favorable core units due to their inherent high-charge transport characteristics. This can be accredited to the extensive π -conjugated system and coplanar molecular structure resulting from π -orbital overlap [33–35]. Moreover, the sulfur-rich nature of fused thiophenes leads to strong intermolecular interactions between adjacent molecules, enhancing the efficient dimensionality of the molecule and improving charge transfer characteristics [36,37]. Additionally, fused thiophenes with a large band gap have been utilized in diverse thiophene-based OSCs, demonstrating enhanced air stability [38–40]. Among these, OSCs utilizing the BTT structure have shown reliable electrical performance in ambient environments [41–46]. For instance, Huang et al. proposed BBTT, a dimer of BTT semiconductors, and OFET based on BBTT exhibited decent electrical properties with a hole mobility of $0.22 \text{ cm}^2/\text{Vs}$ [38]. Mathis group suggested BTT compounds connected by a phenylene π -bridge spacer as p-type semiconductors, and the fabricated devices demonstrated good charge carrier mobility of $1.0 \text{ cm}^2/\text{Vs}$ with no deterioration even after several months [44]. Moreover, the Youn group suggested novel BTT-based compounds in possession of various core sizes and investigated the correlation between the electrical natures and the molecular structure of BTT composites with maximum mobility of $0.34 \text{ cm}^2/\text{Vs}$ [46].

In this investigation, we propose the synthesis of newly developed solution-processable small-molecule OSCs on the basis of the BTT unit: 2-(benzo[*b*]thieno[2,3-*d*]thiophen-2-yl)dibenzo[*b,d*]thiophene (compound **2**) and 2-(benzo[*b*]thiophen-6-yl)benzo[*b*]thieno[2,3-*d*]thiophene (compound **3**) (Scheme 1). Compound **2** has an extra fused benzene ring compared to compound **3**, allowing us to explore the impact of extended π -conjugation on the physicochemical characteristics of the organic semiconductor. The newly synthesized organic compounds were characterized using various techniques. Thermogravimetric analysis (TGA), differential scanning calorimetry (DSC), UV-vis spectroscopy, and cyclic voltammetry (CV) were used to measure their thermal, optical, and electrochemical properties. Density functional theory (DFT) calculations were applied to determine the frontier molecular orbital structure and energy of the synthesized materials. Additionally, atomic force microscopy (AFM) and X-ray diffraction (XRD) were utilized to examine the morphology and microstructure of solution-processed thin films of the organic semiconductors. We made up bottom-gate/top-contact OFETs using the solution-shearing method. Our results demonstrate that both compounds exhibit p-type characteristics as small-molecule organic semiconductors. Notably, OFETs incorporating compound **3** as the semiconductor layer revealed a high carrier mobility of $0.005 \text{ cm}^2/\text{Vs}$ and an on/off current ratio exceeding 10^6 .



Scheme 1. Schematic representation of the synthesis process for compounds 2 and 3.

2. Experimental

2.1. General Substances and Procedures

To conduct air and/or moisture-sensitive reactions, a controlled environment was created using an argon atmosphere. All glassware used was thoroughly dried in an oven, and anhydrous solvents were employed. Unless stated otherwise, commercially available compounds were utilized without additional purification. Solvents were either freshly distilled or dehydrated by moving through an alumina column. Synthesized composites were analyzed by following the previously reported method outlined in the former work [47].

TGA was implemented in a nitrogen (N_2) atmosphere by heating two compounds from 40 to 700 °C. DSC was performed at a speed of 10 °C/min from 30 to 260 °C under a nitrogen flow of 20 mL/min to characterize the thermal features of novel BTT-based compounds. UV-Vis analysis using dilute chloroform solvent was done to investigate the optical features of the two composites. Electrochemical features of the substances were identified by CV utilizing tetra butyl ammonium perchlorate as the supporting electrolyte and ferrocene/ferrocenium as the reference.

2.2. Synthesis

2.2.1. Synthesis of Benzo[*b*]thieno[2,3-*d*]thiophen-2-yltributylstannane (1)

A solution containing 300.0 mg (1.58 mmol) of benzo[*b*]thieno[2,3-*d*]thiophene in 20 mL of tetrahydrofuran (THF) was cooled down to $-78\text{ }^{\circ}\text{C}$ in a nitrogen atmosphere, and then 0.694 mL (1.73 mmol) of *n*-BuLi (2.5 M in *n*-hexane) was supplemented dropwise over a period of 15 min to the reaction compound at $-78\text{ }^{\circ}\text{C}$. The resulting blend was stirred at $-78\text{ }^{\circ}\text{C}$ for 1 h, followed by stirring at $-40\text{ }^{\circ}\text{C}$ for 30 min. After returning to $-78\text{ }^{\circ}\text{C}$, 0.428 mL (1.58 mmol) of tributyltin chloride was supplemented, and the solution was stirred at room temperature for 24 h. The reaction was extinguished by the extra 10 mL of water, and the organic compound obtained was extracted with CH_2Cl_2 . The organic phase was desiccated with anhydrous MgSO_4 and concentrated at reduced pressure. The resulting green oil was further refined through distillation under low pressure. Compound 1 was used without further purification [41].

2.2.2. Preparation of 2-(benzo[*b*]thieno[2,3-*d*]thiophen-2-yl)dibenzo[*b,d*]thiophene (2)

A solution containing 177.0 mg (0.37 mmol) of compound 1, 81.0 mg (0.12 mmol) of 2-bromodibenzo[*b,d*]thiophene, and 7.1 mg (0.006 mmol) of $\text{Pd}(\text{PPh}_3)_4$ in 30 mL of toluene was stirred at $120\text{ }^{\circ}\text{C}$ for 16 h in a nitrogen atmosphere. After returning to room temperature, the blend was extracted with CH_2Cl_2 and desiccated using anhydrous MgSO_4 . The solvent was then subjected to vacuum evaporation, and the resulting residue was refined by crystallization employing hexane to yield compound 2 as a yellow solid (36.3 mg, 79.2%). ^1H NMR (400 MHz, CDCl_3): δ 8.40 (d, $J = 1.8\text{ Hz}$, 1H), 8.24–8.19 (m, 1H), 7.88–7.81 (m, 4H), 7.77–7.74 (m, 1H), 7.63–7.60 (m, 1H), 7.52–7.46 (m, 2H), 7.45–7.32 (m, 2H). ^{13}C NMR (101 MHz, CDCl_3): δ 147.2, 142.3, 140.1, 139.2, 138.8, 136.3, 135.3, 133.8, 132.9, 131.2, 127.2, 124.9, 124.8, 124.7, 124.5, 124.0, 123.4, 123.1, 121.8, 121.0, 118.8, 116.3. HRMS-EI (m/z): [$\text{M} + \text{H}^+$] calculated for $\text{C}_{22}\text{H}_{13}\text{S}_3$, 373.0174; found, 373.0176 (Figure S1).

2.2.3. Preparation of 2-(benzo[*b*]thiophen-6-yl)benzo[*b*]thieno[2,3-*d*]thiophene (3)

A solution containing 331.3 mg (0.69 mmol) of compound 1, 147.2 mg (0.69 mmol) of 6-bromobenzo[*b*]thiophene, and 39.9 mg (0.03 mmol) of $\text{Pd}(\text{PPh}_3)_4$ in 30 mL of toluene was stirred at $120\text{ }^{\circ}\text{C}$ for 16 h in a nitrogen atmosphere. After returning to room temperature, the blend was extracted with CH_2Cl_2 and desiccated employing anhydrous MgSO_4 . The solvent was eliminated under vacuum conditions, and the resulting residue was refined by crystallization employing hexane to yield compound 3 as a yellow solid (101.9 mg, 45.6%). ^1H NMR (400 MHz, CDCl_3): δ 8.16 (t, $J = 0.9\text{ Hz}$, 1H), 7.83 (t, $J = 8.9\text{ Hz}$, 3H), 7.68 (dd, $J = 8.5, 1.6\text{ Hz}$, 1H), 7.58 (s, 1H), 7.48–7.46 (m, 1H), 7.43–7.31 (m, 3H). ^{13}C NMR (101 MHz, CDCl_3): δ 147.2, 142.3, 140.7, 139.4, 138.8, 132.9, 130.9, 129.1, 127.4, 124.9, 124.5, 124.1, 123.9, 123.8, 122.8, 121.0, 119.6, 116.3. HRMS-EI (m/z): [$\text{M} + \text{H}^+$] calculated for $\text{C}_{18}\text{H}_{11}\text{S}_3$, 323.0017; found, 323.0022 (Figure S1).

2.3. Theoretical Calculation

The synthesized compounds underwent DFT calculations utilizing the B3LYP (Becke's 3 parameters, the Lee-Yang-Parr) method with a 6–31 G(d) basis set, which was performed in the Gaussian 09W program.

2.4. Device Production

The bottom-gate/top-contact architecture utilized highly *n*-doped (100) silicon wafers with a resistivity of less than $0.005\ \Omega\ \text{cm}$ as substrates. These substrates had a thermally grown SiO_2 gate dielectric layer that was 300 nm thick with an areal capacitance of $11.4\ \text{nF}/\text{cm}^2$. Prior to the fabrication process, the substrates underwent a 15 min sonication in acetone and isopropyl alcohol (IPA) and a 10 min exposure to O_2 plasma using a Harrick Plasma system operating at 18 W in succession. The gate dielectric layers were treated with a hydroxyl-functionalized polystyrene (PS-brush) treatment. A solution of toluene containing 0.5 wt% PS-brush with a molecular weight of 32,000 g/mol was applied

to Si/SiO₂ substrates utilizing spin-coating at a rotation rate of 3000 rpm for a duration of 30 s. Afterward, the substrates underwent thermal annealing in a vacuum oven at a temperature of 70 °C for a duration of 48 h. Subsequently, they were cleaned with toluene and annealed at 100 °C for 24 h. [47]. The active layers based on BTT were developed using the solution-shearing (SS) technique with diverse solvents, shearing speeds, and annealing temperatures to enhance semiconductor performance. After the solution process, the solution-sheared films underwent annealing at an identical temperature to that of the shearing temperature to get rid of any residual solution. The source and drain electrodes were produced via thermally evaporating a 30 nm layer of gold at a deposition speed of 0.2 Å/s through a shadow mask with a channel length of 100 μm and a width of 500 μm.

2.5. Device and Film Characterization

The transfer and output characteristics of OTFT devices were evaluated by employing a Keithley 4200 model semiconductor parameter analyzer in ambient environments. Hole mobilities in the saturated region (μ_{sat}) were calculated via following equation, $\mu_{\text{sat}} = (2I_{\text{DS}}L)/[WC_i(V_G - V_T)^2]$, where I_{DS} represents the current flowing between the source and drain electrodes, L means the channel length, W means the channel width, C_i means the capacitance per area of the gate dielectric (11.4 nF/cm²), V_G means the gate voltage, and V_T means the threshold voltage. The surface morphology and microstructure of the thin films were evaluated utilizing an atomic force microscope (AFM), specifically the Park System XE 7 model in non-contact mode, and an X-ray diffractometer (XRD), specifically the Bruker D8 Advance model.

3. Results and Discussion

3.1. Synthesis

Benzo[*b*]thieno[2,3-*d*]thiophen-2-yltributylstannane (**1**) was synthesized through stannylation and used immediately. Then, Stille coupling of compound **1** with a compatible aryl bromide resulted in the formation of 2-(benzo[*b*]thieno[2,3-*d*]thiophen-2-yl)dibenzo[*b,d*]thiophene (**2**), and 2-(benzo[*b*]thiophen-6-yl)benzo[*b*]thieno[2,3-*d*]thiophene (**3**) as illustrated in Scheme 1.

3.2. Thermal, Optical, and Electrochemical Features of Synthesized Compounds

TGA and DSC were performed to obtain the thermal characteristics of novel synthesized materials (Figures S2 and S3). For compounds **2** and **3**, TGA plots exhibited the onset temperatures of 5% weight loss to be 281 °C and 248 °C, respectively, representing excellent thermal stability of BTT compounds (Table 1). Compound **3** features a benzothiophene functional group added to the BTT unit, while compound **2** incorporates a dibenzothiophene functional group into the BTT unit. The dibenzothiophene functional group introduces additional C-C bonds, which may require supplementary thermal energy for their breakage [48,49]. As a result, compound **2** exhibited higher thermal decomposition temperature compared to compound **3**. The melting temperatures (T_m) of both composites were determined to be similar to 194 °C and 191 °C, respectively, based on DSC measurements (Table 1).

Table 1. Physical and electrochemical characteristics of BTT composites.

	T_d (°C) ^a	T_m (°C) ^b	λ_{max} (nm) ^c		λ_{onset} (nm) ^c	E_{gap} (eV) ^c	$E_{\text{ox}}^{\text{onset}}$ (V) ^d	E_{HOMO} (eV) ^d	E_{LUMO} (eV) ^e
			Solution	Film					
2	281	194	335	311	384	3.23	1.16	−5.49	−2.26
3	248	191	350	328	385	3.22	1.18	−5.51	−2.29

^a Decomposition temperature (5% weight loss) and ^b melting temperature. ^c Calculated from UV-vis spectra.

^d Calculated by CV in dichloromethane at room temperature (using ferrocene/ferrocenium as internal standard) and E_{ox} = oxidation potential. ^e $E_{\text{LUMO}} = E_{\text{HOMO}} + E_{\text{gap}}$.

To investigate the optical characteristics, UV-Vis absorption spectra of compounds 2–3 in diluted chloroform solution were acquired. The onset absorption wavelengths (λ_{onset}) of compounds 2 and 3 in the chloroform solution were determined as 384 and 385 nm, respectively (Figure 1). Therefore, the band gaps (E_g) of the organic semiconductors obtained from the onset of the UV-Vis absorption spectra were almost the same (3.22–3.23 eV). The maximum absorption wavelengths (λ_{max}) of compounds 2–3 in chloroform solution were observed at 335 nm and 350 nm, respectively. On the other hand, when deposited as thin films on a glass substrate, the maximum absorption wavelengths (λ_{max}) of compounds 2–3 revealed a blue shift, with peak values at 311 nm and 328 nm, respectively (Figure S4). This observed blue shift in the thin film absorption spectra, in comparison with their solution absorption spectra, can be attributed to the formation of H-aggregation within the thin films [50].

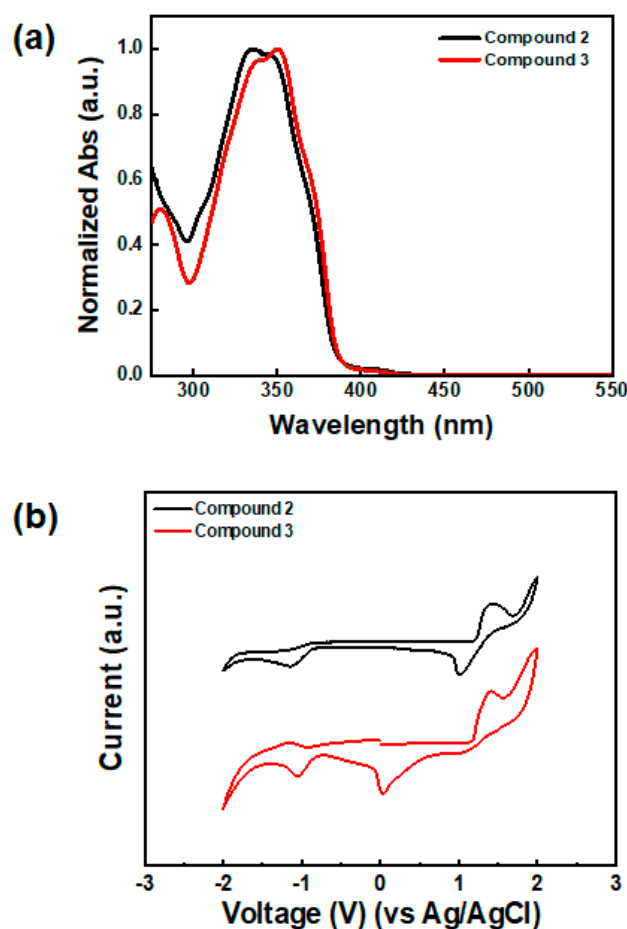


Figure 1. (a) UV-Vis absorption spectra of compounds 2–3 dissolved in chloroform and (b) CV curves of compounds 2–3 using dichloromethane as the solvent at room temperature.

CV experiments were implemented in a dichloromethane solution at room temperature to evaluate the HOMO and LUMO levels of compounds 2–3 (Figure 1). The oxidation peaks of compounds 2 and 3 were found at 1.16 and 1.18 V. The HOMO level was estimated utilizing the ferrocene/ferrocenium internal standard and the regular equation:

$$E_{\text{HOMO}}(\text{eV}) = 4.8\text{eV} - e(E_{\text{ox}}^{\text{onset}} - E_{\text{FC}/\text{FC}^+}^{\text{onset}}) \quad (1)$$

where $E_{\text{ox}}^{\text{onset}}$ represents the onset of oxidation potential. Thus, the HOMO energy levels were measured as -5.49 and -5.51 eV for compounds 2 and 3, respectively. The LUMO levels were obtained from the variation between the HOMO levels and the band gap energy estimated from UV-Vis spectroscopy, affording -2.26 and -2.29 eV for compounds 2 and 3,

respectively. Although compound **2** contains an additional benzene ring, both compounds showed similar HOMO/LUMO energy levels.

3.3. Theoretical Calculation

DFT calculations were implemented employing the Gaussian 09W program (B3LYP with 6-31 G(d) basis sets) to identify the HOMO/LUMO energy distribution of the newly synthesized materials. Figure 2 illustrates that the HOMO and LUMO orbitals of compound **3** are distributed throughout the BTT unit, whereas those of compound **2** do not cover the terminal benzene ring. This result is in accordance with the experimentally obtained HOMO/LUMO energy levels (*vide supra*). Hence, the estimated theoretical HOMO and LUMO levels of the two composites were similar as $-5.34/-1.54$ eV for compound **2** and $-5.33/-1.64$ eV for compound **3**. The estimated theoretically optimized molecular constitutions of compounds **2–3** exhibited dihedral angles of -180° , obviously indicating the planarity of these organizations (Figure S5).

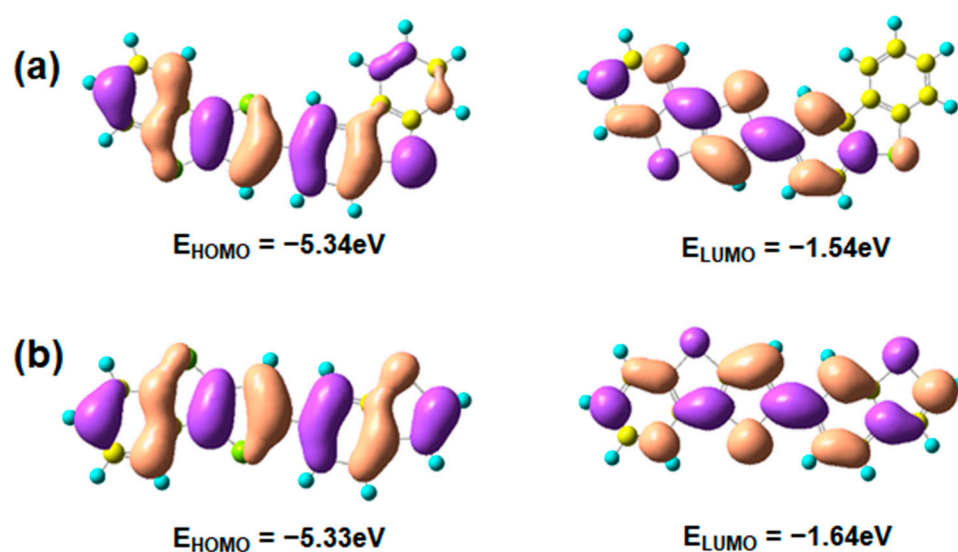


Figure 2. Calculated orbital diagrams and energy levels of the HOMO/LUMO energy levels for (a) compound **2** and (b) compound **3**.

3.4. Characterization of the Microstructure and Morphology of the Thin-Films

The microstructure and surface morphology of the fabricated thin films were characterized using θ - 2θ XRD analysis and AFM analysis. Figure 3 represents the XRD profile of the thin film of compound **3**, revealing multiple diffraction peaks with significant peak intensity, which demonstrates the highly ordered microstructure of films [51] compared to those of compound **2**. In contrast, XRD profiles of a thin film of compound **2** displayed feeble (001) reflection, suggesting a relatively lower degree of crystalline ordering in comparison with that of compound **3** [52,53]. In addition, we could estimate the film microstructures of compounds **2–3** by comparing the full width of half maximum (FWHM) values of their XRD profiles. The (001) peak FWHMs for compounds **2** and **3** were 0.13° and 0.07° , respectively, which indicates that the grain size of compound **3** is larger than compound **2**. This outcome represents that the intermolecular ordering was reduced by the additional benzene ring, which might increase the steric hindrance that undermines intermolecular van der Waals interactions [54]. The prominent primary diffraction peaks in the thin films of compounds **2** and **3** were observed at $2\theta = 5.66^\circ$ and 5.90° , consistent with calculated d-spacings of 1.56 nm and 1.50 nm. Notably, the theoretical molecular lengths of compounds **2** and **3** are 1.59 nm and 1.51 nm. This implies that both compounds exhibit a vertically aligned molecular arrangement on the film surface, as their d-spacing values closely match their respective molecular lengths [38,46].

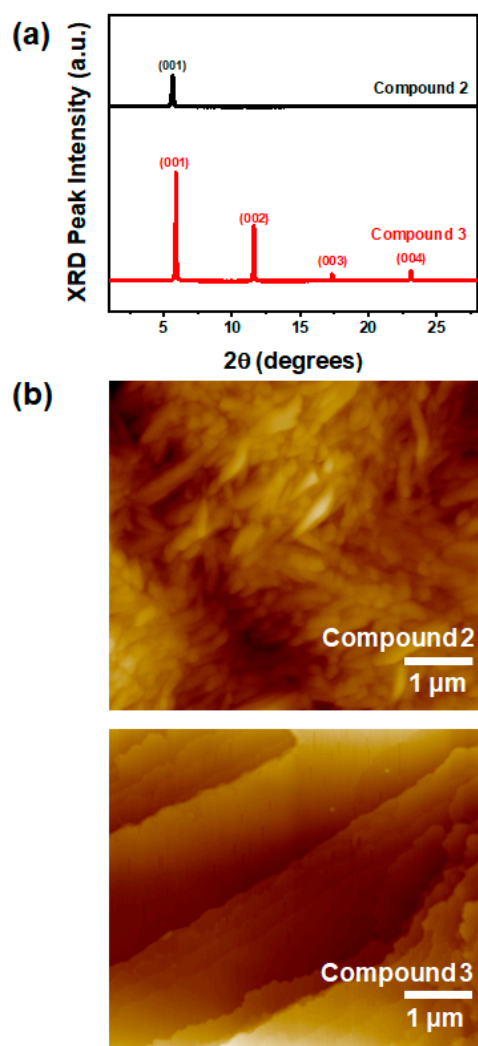


Figure 3. (a) X-ray diffraction profiles and (b) AFM images ($5 \times 5 \mu\text{m}$) of the thin films fabricated by compounds 2–3.

To assess the film morphology, a non-contact mode AFM analysis was conducted on thin films of organic semiconductors (OSCs) utilizing compounds 2 and 3 (Figure 3). The surface morphology of the compound 2 film revealed the presence of small, rod-shaped grains with a substantial number of grain boundaries. It is noteworthy that the presence of large grain boundaries and small grains is indicative of limited interconnectivity, which can lead to compromised charge transport characteristics within the film [55,56]. Surface morphology analysis of thin films of compound 3 revealed larger grains and featured continuous terraced layers and relatively smooth surface coverage, which could lead to a better electrical performance in comparison with compound 2 (vide infra) [57,58].

3.5. Field-Effect Transistor Characterization

OFETs were fabricated utilizing the solution-shearing technique employing two newly developed BTT-based compounds as active layers. The devices were tested under atmospheric conditions to evaluate their electrical performance. To optimize the solution-shearing process several parameters inclusive of a solvent kind, concentration, substrate annealing temperature, and shearing rate were adjusted. The resulting electrical performance parameters, inclusive of average hole mobilities, current on/off ratio, and threshold voltages, were recorded and tabulated in Table 2 for comprehensive analysis and summary. Among the devices, the OFET utilizing compound 3 as the semiconductor layer revealed the highest electrical performance, with carrier mobility as high as $0.005 \text{ cm}^2/\text{Vs}$ and a

current on/off ratio $> 10^6$ (Figure 4), consistently with film microstructure and morphology analysis (vide supra). Compound 2 displayed lower electrical performance with carrier mobility $\sim 10\times$ lower than that based on compound 3 (Figure S6).

Table 2. OFET performance employing thin films of BTT composites.

Compound	μ^{avg} (cm^2/Vs) (μ^{max} (cm^2/Vs))	$I_{\text{on}}/I_{\text{off}}$	V_{th} (V)
2	0.0003 ± 0.0001 (0.0003)	$(1.0 \pm 0.3) \times 10^5$	-3 ± 1.0
3	0.0045 ± 0.0005 (0.005)	$(1.7 \pm 0.5) \times 10^6$	-5 ± 1.0

μ : charge carrier mobility, $I_{\text{on}}/I_{\text{off}}$: current on/off ratio, V_{th} : threshold voltage. The average values of each parameter were estimated from 12 devices in ambient conditions.

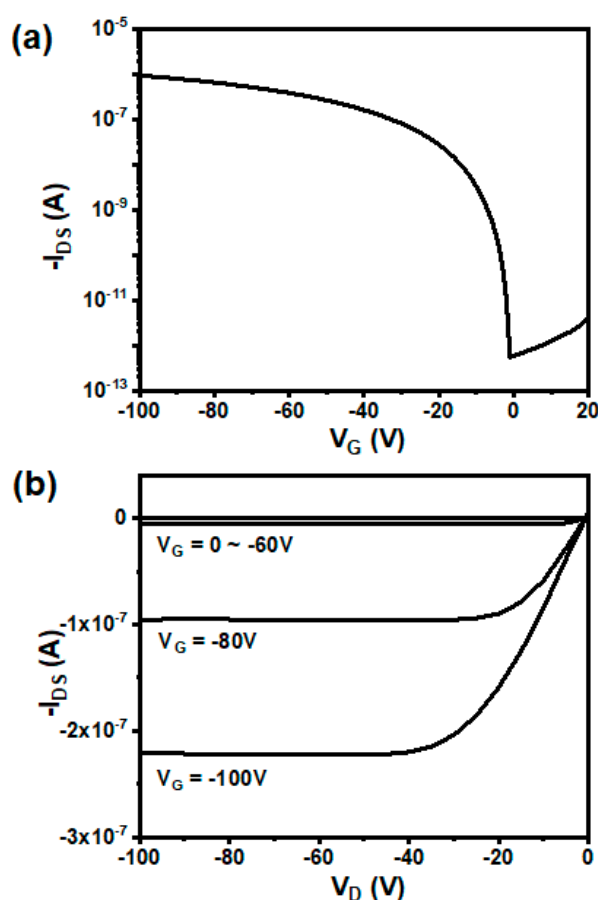


Figure 4. (a) The transfer properties and (b) output properties of OFETs using BTT-derivative (compound 3).

4. Conclusions

In brief, we have successfully synthesized and described fresh derivatives of benzo[*b*]thieno[2,3-*d*]thiophene (BTT). Comprehensive analyses, including TGA, DSC, UV-vis spectroscopy, CV, and DFT, were performed to investigate their physicochemical properties. The fabricated field-effect transistor devices demonstrated p-channel behavior in the ambient environment. Particularly, compound 3 exhibited the highest mobility, reaching up to $0.005 \text{ cm}^2/\text{Vs}$, and a current on/off ratio exceeding 10^6 in the ambient condition. Moreover, XRD and AFM measurements of compound 3 displayed highly crystalline films with well-defined terraced layers. Our research involves the synthesis of BTT-based compounds with different structures and aims to systematically screen their properties. Through this study, further

research on the development of fused thiophene derivatives with various substituents is underway.

Supplementary Materials: The following supporting information can be downloaded at <https://www.mdpi.com/article/10.3390/coatings13081417/s1>, Figure S1: (a) H NMR, (b) C NMR, (c) Q-TOF MS spectra of compound **2**, (d) H NMR, (e) C NMR, (c) Q-TOF MS spectra of compound **3**; Figure S2: Thermogravimetric analysis of (a) compound **2** and (b) compound **3**; Figure S3: Differential scanning calorimetry of (a) compound **2** and (b) compound **3**; Figure S4: UV-vis absorption spectra of compounds **2–3** as thin films on glass substrate; Figure S5: Optimized conjugated backbone planarity of compounds **2–3** obtained by DFT calculation (dihedral angle = -180°); Figure S6: Transfer curve including the hysteresis of scanning of the OFETs based on (a) compound **3** (b) compound **2**.

Author Contributions: Conceptualization, C.K. and S.S.; Validation, C.K.; Investigation, S.K., S.R., J.A., C.K. and S.S.; Data curation, S.K., S.R. and J.A.; Writing—original draft, S.K. and S.R.; Writing—review & editing, D.K., A.M., C.K. and S.S.; Visualization, S.R. and J.A.; Supervision, C.K. and S.S.; Funding acquisition, S.S. All authors have read and agreed to the published version of the manuscript.

Funding: This research was supported by the National Research Foundation of Korea (NRF) grant funded by the Korea government (NRF-2021R1F1A1050933, RS-2022-00142063).

Institutional Review Board Statement: Not applicable.

Informed Consent Statement: Not applicable.

Data Availability Statement: All data that support the findings of this study are included within the article.

Conflicts of Interest: The authors state that they have no known conflict of interest or personal relationships that could have influenced the work reported in this paper.

References

1. Arias, A.C.; MacKenzie, J.D.; McCulloh, I.; Rivnay, J.; Salleo, A. Materials and applications for large area electronics: Solution-based approaches. *Chem. Rev.* **2010**, *110*, 3–24. [[CrossRef](#)] [[PubMed](#)]
2. Berggren, M.; Nilsson, D.; Robinson, N.D. Organic materials for printed electronics. *Nat. Mater.* **2007**, *6*, 3–5. [[CrossRef](#)]
3. Brütting, W. *Introduction to the Physics of Organic Semiconductors*; Physics of Organic Semiconductors: Weinheim, Germany, 2005; pp. 1–14.
4. Caironi, M.; Noh, Y.-Y. *Large Area and Flexible Electronics*; John Wiley & Sons: Hoboken, NJ, USA, 2015.
5. Mamada, M.; Shima, H.; Yoneda, Y.; Shimano, T.; Yamada, N.; Kakita, K.; Machida, T.; Tanaka, Y.; Aotsuka, S.; Kumaki, D.; et al. A unique solution-processable n-type semiconductor material design for high-performance organic field-effect transistors. *Chem. Mater.* **2015**, *27*, 141–147. [[CrossRef](#)]
6. Ozdemir, M.; Choi, D.; Kwon, G.; Zorlu, Y.; Cosut, B.; Kim, H.; Facchetti, A.; Kim, C.; Usta, H. Solution-processable BODIPY-based small molecules for semiconducting microfibers in organic thin-film transistors. *ACS Appl. Mater. Interfaces* **2016**, *8*, 14077–14087. [[CrossRef](#)] [[PubMed](#)]
7. Ruiz, C.; Garcia-Frutos, E.M.; Hennrich, G.; Gómez-Lor, B. Organic semiconductors toward electronic devices: High mobility and easy processability. *J. Phys. Chem. Lett.* **2012**, *3*, 1428–1436. [[CrossRef](#)] [[PubMed](#)]
8. Sun, Y.; Liu, Y.; Zhu, D. Advances in organic field-effect transistors. *J. Mater. Chem.* **2005**, *15*, 53–65. [[CrossRef](#)]
9. Cheng, P.; Li, G.; Zhan, X.; Yang, Y. Next-generation organic photovoltaics based on non-fullerene acceptors. *Nat. Photonics* **2018**, *12*, 131–142. [[CrossRef](#)]
10. Facchetti, A. Semiconductors for organic transistors. *Mater. Today* **2007**, *10*, 28–37. [[CrossRef](#)]
11. Huang, F.; Yip, H.-L.; Cao, Y. *Polymer Photovoltaics: Materials, Physics, and Device Engineering*; Royal Society of Chemistry: London, UK, 2015.
12. Lee, S.-H.; Park, H.-L.; Kang, S.; Kim, M.-H.; Lee, S.D. Organic thin-film transistors with liquid crystalline polymer insulator integrated for solution-processed organic light-emitting devices. *Semicond. Sci. Technol.* **2019**, *34*, 105012. [[CrossRef](#)]
13. Lin, P.; Yan, F. Organic thin-film transistors for chemical and biological sensing. *Adv. Mater.* **2012**, *24*, 34–51. [[CrossRef](#)]
14. Murphy, A.R.; Frechet, J.M. Organic semiconducting oligomers for use in thin film transistors. *Chem. Rev.* **2007**, *107*, 1066–1096. [[CrossRef](#)] [[PubMed](#)]
15. Reese, C.; Roberts, M.; Ling, M.; Bao, Z. Organic thin film transistors. *Mater. Today* **2004**, *7*, 20–27. [[CrossRef](#)]
16. Tang, M.L.; Okamoto, T.; Bao, Z. High-performance organic semiconductors: Asymmetric linear acenes containing sulphur. *J. Am. Chem. Soc.* **2006**, *128*, 16002–16003. [[CrossRef](#)]
17. Torsi, L.; Magliulo, M.; Manoli, K.; Palazzo, G. Organic field-effect transistor sensors: A tutorial review. *Chem. Soc. Rev.* **2013**, *42*, 8612–8628. [[CrossRef](#)] [[PubMed](#)]

18. Feng, S.; Duan, L.; Hou, L.; Qiao, J.; Zhang, D.; Dong, G.; Wang, L.; Qiu, Y. A comparison study of the organic small molecular thin films prepared by solution process and vacuum deposition: Roughness, hydrophilicity, absorption, photoluminescence, density, mobility, and electroluminescence. *J. Phys. Chem. C* **2011**, *115*, 14278–14284. [[CrossRef](#)]
19. Xing, X.; Zhong, L.; Zhang, L.; Chen, Z.; Qu, B.; Chen, E.; Xiao, L.; Gong, Q. Essential differences of organic films at the molecular level via vacuum deposition and solution processes for organic light-emitting diodes. *J. Phys. Chem. C* **2013**, *117*, 25405–25408. [[CrossRef](#)]
20. Diao, Y.; Tee, B.C.-K.; Giri, G.; Xu, J.; Kim, D.H.; Becerril, H.A.; Stoltenberg, R.M.; Lee, T.H.; Xue, G.; Mannsfeld, S.C.B.; et al. Solution coating of large-area organic semiconductor thin films with aligned single-crystalline domains. *Nat. Mater.* **2013**, *12*, 665–671. [[CrossRef](#)]
21. Shaw, L.; Bao, Z. The Large-Area, Solution-Based Deposition of Single-Crystal Organic Semiconductors. *Isr. J. Chem.* **2014**, *54*, 496–512. [[CrossRef](#)]
22. Ling, M.M.; Gomez, M.; Koenemann, M.; Locklin, J.; Bao, Z. Air-stable n-channel organic semiconductors based on perylene diimide derivatives without strong electron withdrawing groups. *Adv. Mater.* **2007**, *19*, 1123–1127. [[CrossRef](#)]
23. Park, S.K.; Jackson, T.N.; Anthony, J.E.; Mourey, D.A. High mobility solution processed 6, 13-bis (triisopropyl-silylethynyl) pentacene organic thin film transistors. *Appl. Phys. Lett.* **2007**, *91*, 063514. [[CrossRef](#)]
24. Song, D.; Wang, H.; Zhu, F.; Yang, J.; Tian, H.; Geng, Y.; Yan, D. Phthalocyanato Tin (IV) Dichloride: An Air-Stable, High-Performance, n-Type Organic Semiconductor with a High Field-Effect Electron Mobility. *Adv. Mater.* **2008**, *20*, 2142–2144. [[CrossRef](#)]
25. Tian, H.K.; Shi, J.W.; Yan, D.H.; Wang, L.X.; Geng, Y.H.; Wang, F.S. Naphthyl End-Capped Quarterthiophene: A Simple Organic Semiconductor with High Mobility and Air Stability. *Adv. Mater.* **2006**, *18*, 2149–2152. [[CrossRef](#)]
26. Zschieschang, U.; Ante, F.; Yamamoto, T.; Takimiya, K.; Kuwabara, H.; Ikeda, M.; Sekitani, T.; Someya, T.; Kern, K.; Klauk, H. Flexible low-voltage organic transistors and circuits based on a high-mobility organic semiconductor with good air stability. *Adv. Mater.* **2010**, *22*, 982–985. [[CrossRef](#)]
27. Lim, B.; Sun, H.; Noh, Y.-Y. Highly soluble small-molecule organic semiconductor with trihexylsilyloxy side chain for high-performance organic field-effect transistors with mobility of up to $3.10 \text{ cm}^2 \text{ V}^{-1} \text{ s}^{-1}$. *Dye. Pigment.* **2017**, *142*, 17–23. [[CrossRef](#)]
28. Liu, Z.; Zhang, G.; Cai, Z.; Chen, X.; Luo, H.; Li, Y.; Wang, J.; Zhang, D. New organic semiconductors with imide/amide-containing molecular systems. *Adv. Mater.* **2014**, *26*, 6965–6977. [[CrossRef](#)] [[PubMed](#)]
29. Vegiraju, S.; Hsieh, C.-M.; Huang, D.-Y.; Chen, Y.-C.; Priyanka, P.; Ni, J.-S.; ESYA, F.A.; Kim, C.; Yau, S.L.; Chen, C.-P.; et al. Synthesis and characterization of solution-processable diketopyrrolopyrrole (DPP) and tetrathienothiophene (TTA)-based small molecules for organic thin film transistors and organic photovoltaic cells. *Dye. Pigment.* **2016**, *133*, 280–291. [[CrossRef](#)]
30. Wang, C.; Dong, H.; Hu, W.; Liu, Y.; Zhu, D. Semiconducting π -conjugated systems in field-effect transistors: A material odyssey of organic electronics. *Chem. Rev.* **2012**, *112*, 2208–2267. [[CrossRef](#)]
31. Yakuphanoglu, F.; Aydin, M.; Arsu, N.; Sekerci, M. A small-molecule organic semiconductor. *Semiconductors* **2004**, *38*, 468–471. [[CrossRef](#)]
32. Youn, J.; Vegiraju, S.; Emery, J.D.; Leever, B.J.; Kewalramani, S.; Lou, S.J.; Zhang, S.; Prabakaran, K.; Ezhumalai, Y.; Kim, C.; et al. Dipierfluorophenyl fused thiophene semiconductors for n-type organic thin film transistors (OTFTs). *Adv. Electron. Mater.* **2015**, *1*, 1500098. [[CrossRef](#)]
33. Ashraf, R.S.; Gilot, J.; Janssen, R.A. Fused ring thiophene-based poly (heteroarylene ethynylene) s for organic solar cells. *Sol. Energy Mater. Sol. Cells* **2010**, *94*, 1759–1766. [[CrossRef](#)]
34. Kumaresan, P.; Vegiraju, S.; Ezhumalai, Y.; Yau, S.L.; Kim, C.; Lee, W.-H.; Chen, M.-C. Fused-thiophene based materials for organic photovoltaics and dye-sensitized solar cells. *Polymers* **2014**, *6*, 2645–2669. [[CrossRef](#)]
35. Lu, R.-Q.; Zhou, Y.-N.; Yan, X.-Y.; Shi, K.; Zheng, Y.-Q.; Luo, M.; Wang, X.-C.; Pei, J.; Xia, H.; Zoppi, L.; et al. Thiophene-fused bowl-shaped polycyclic aromatics with a dibenzo [a, g] corannulene core for organic field-effect transistors. *Chem. Commun.* **2015**, *51*, 1681–1684. [[CrossRef](#)] [[PubMed](#)]
36. Wu, W.; Liu, Y.; Zhu, D. π -Conjugated molecules with fused rings for organic field-effect transistors: Design, synthesis and applications. *Chem. Soc. Rev.* **2010**, *39*, 1489–1502. [[CrossRef](#)]
37. Yang, K.; Liao, Q.; Koh, C.W.; Chen, J.; Su, M.; Zhou, X.; Tang, Y.; Wang, Y.; Zhang, Y.; Woo, H.Y.; et al. Improved photovoltaic performance of a nonfullerene acceptor based on a benzo [b] thiophene fused end group with extended π -conjugation. *J. Mater. Chem. A* **2019**, *7*, 9822–9830. [[CrossRef](#)]
38. Huang, P.-Y.; Chen, L.-H.; Chen, Y.-Y.; Chang, W.-J.; Wang, J.-J.; Lii, K.-H.; Yan, J.-Y.; Ho, J.-C.; Lee, C.-C.; Kim, C.; et al. Enhanced Performance of Benzothieno [3, 2-b] thiophene (BTT)-Based Bottom-Contact Thin-Film Transistors. *Chem.–A Eur. J.* **2013**, *19*, 3721–3728. [[CrossRef](#)]
39. Ra, C.-S.; Yim, S.-G.; Park, G.-S. DFT studies of band gaps of the fused thiophene oligomers. *Bull. Korean Chem. Soc.* **2008**, *29*, 891–893.
40. Takimiya, K.; Ebata, H.; Sakamoto, K.; Izawa, T.; Otsubo, T.; Kunugi, Y. 2, 7-Diphenyl [1] benzothieno [3, 2-b] benzothiophene, a new organic semiconductor for air-stable organic field-effect transistors with mobilities up to $2.0 \text{ cm}^2 \text{ V}^{-1} \text{ s}^{-1}$. *J. Am. Chem. Soc.* **2006**, *128*, 12604–12605. [[CrossRef](#)]

41. Chen, H.; Cui, Q.; Yu, G.; Guo, Y.; Huang, J.; Zhu, M.; Guo, X.; Liu, Y. Synthesis and characterization of novel semiconductors based on thieno [3, 2-b][1] benzothiophene cores and their applications in the organic thin-film transistors. *J. Phys. Chem. C* **2011**, *115*, 23984–23991. [[CrossRef](#)]
42. Hyodo, K.; Hagiwara, H.; Toyama, R.; Mori, H.; Soga, S.; Nishihara, Y. Bis [1] benzothieno [2, 3-d: 2', 3'-d'] anthra [1, 2-b: 5, 6-b'] dithiophene: Synthesis, characterization, and application to organic field-effect transistors. *RSC Adv.* **2017**, *7*, 6089–6092. [[CrossRef](#)]
43. Liu, Y.; Liu, Z.; Luo, H.; Xie, X.; Ai, L.; Ge, Z.; Yu, G.; Liu, Y. Benzothieno [2, 3-b] thiophene semiconductors: Synthesis, characterization and applications in organic field-effect transistors. *J. Mater. Chem. C* **2014**, *2*, 8804–8810. [[CrossRef](#)]
44. Mathis, T.; Liu, Y.; Ai, L.; Ge, Z.; Lumpi, D.; Horkel, E.; Holzer, B.; Froehlich, J.; Batlogg, B. Stable organic field-effect-transistors with high mobilities unaffected by supporting dielectric based on phenylene-bridged thienobenzothiophene. *J. Appl. Phys.* **2014**, *115*, 043707. [[CrossRef](#)]
45. Wang, L.; Li, T.; Shen, Y.; Song, Y. A theoretical study of the electronic structure and charge transport properties of thieno [2, 3-b] benzothiophene based derivatives. *Phys. Chem. Chem. Phys.* **2016**, *18*, 8401–8411. [[CrossRef](#)] [[PubMed](#)]
46. Youn, J.; Huang, P.-Y.; Zhang, S.; Liu, C.-W.; Vegiraju, S.; Prabakaran, K.; Stern, S.; Kim, C.; Chen, M.-C.; Facchetti, A.; et al. Functionalized benzothieno [3, 2 b] thiophenes (BTT s) for high performance organic thin-film transistors (OTFTs). *J. Mater. Chem. C* **2014**, *2*, 7599–7607. [[CrossRef](#)]
47. Park, S.; Ryu, S.; Ho, D.; Chae, W.; Earmme, T.; Kim, C.; Seo, S. Novel benzo [b] thieno [2, 3-d] thiophene derivatives with an additional alkyl-thiophene core: Synthesis, characterization, and p-type thin film transistor performance. *New J. Chem.* **2022**, *46*, 12196–12205. [[CrossRef](#)]
48. Niemczak, M.; Rzemieniecki, T.; Sobiech, Ł.; Skrzypczak, G.; Praczyk, T.; Pernak, J. Influence of the alkyl chain length on the physicochemical properties and biological activity in a homologous series of dichlorprop-based herbicidal ionic liquids. *J. Mol. Liq.* **2019**, *276*, 431–440. [[CrossRef](#)]
49. Othman Zailani, N.H.Z.; Yunus, N.M.; Ab Rahim, A.H.; Bustam, M.A. Thermophysical properties of newly synthesized ammonium-based protic ionic liquids: Effect of temperature, anion and alkyl chain length. *Processes* **2020**, *8*, 742. [[CrossRef](#)]
50. Kim, S.O.; An, T.K.; Chen, J.; Kang, I.; Kang, S.H.; Chung, D.S.; Kwon, S. K. H-aggregation strategy in the design of molecular semiconductors for highly reliable organic thin film transistors. *Adv. Funct. Mater.* **2011**, *21*, 1616–1623. [[CrossRef](#)]
51. Ha, T.-J.; Sonar, P.; Dodabalapur, A. Charge transport study of high mobility polymer thin-film transistors based on thiophene substituted diketopyrrolopyrrole copolymers. *Phys. Chem. Chem. Phys.* **2013**, *15*, 9735–9741. [[CrossRef](#)]
52. Chen, S.-C.; Zhang, Q.; Zheng, Q.; Tang, C.; Lu, C.Z. Angular-shaped naphthalene tetracarboxylic diimides for n-channel organic transistor semiconductors. *Chem. Commun.* **2012**, *48*, 1254–1256. [[CrossRef](#)]
53. Kim, H.; Reddy, M.R.; Kwon, G.; Choi, D.; Kim, C.; Seo, S. Synthesis and characterization of 2, 7-diethynyl-benzo [b] benzo [4, 5] thieno [2, 3-d] thiophene derivative as organic semiconductors for organic thin-film transistors. *Synth. Met.* **2016**, *220*, 599–605. [[CrossRef](#)]
54. Nowok, A.; Dulski, M.; Grelska, J.; Szeremeta, A.Z.; Jurkiewicz, K.; Grzybowska, K.; Pawlus, S. Phenyl ring: A steric hindrance or a source of different hydrogen bonding patterns in self-organizing systems? *J. Phys. Chem. Lett.* **2021**, *12*, 2142–2147. [[CrossRef](#)] [[PubMed](#)]
55. Bolognesi, A.; Berliocchi, M.; Manenti, M.; Di Carlo, A.; Lugli, P.; Lmimouni, K.; Dufour, C. Effects of grain boundaries, field-dependent mobility, and interface trap states on the electrical characteristics of pentacene TFT. *IEEE Trans. Electron Devices* **2004**, *51*, 1997–2003. [[CrossRef](#)]
56. Yadav, S.; Kumar, P.; Ghosh, S. Optimization of surface morphology to reduce the effect of grain boundaries and contact resistance in small molecule based thin film transistors. *Appl. Phys. Lett.* **2012**, *101*, 193307. [[CrossRef](#)]
57. Di Carlo, A.; Piacenza, F.; Bolognesi, A.; Stadlober, B.; Maresch, H. Influence of grain sizes on the mobility of organic thin-film transistors. *Appl. Phys. Lett.* **2005**, *86*, 263501. [[CrossRef](#)]
58. Locklin, J.; Bao, Z. Effect of morphology on organic thin film transistor sensors. *Anal. Bioanal. Chem.* **2006**, *384*, 336–342. [[CrossRef](#)] [[PubMed](#)]

Disclaimer/Publisher's Note: The statements, opinions and data contained in all publications are solely those of the individual author(s) and contributor(s) and not of MDPI and/or the editor(s). MDPI and/or the editor(s) disclaim responsibility for any injury to people or property resulting from any ideas, methods, instructions or products referred to in the content.